Title
Radiative sensitivities of tropical anvils to small ice crystals

Journal
Journal of Geophysical Research, 99(D12)

ISSN
0148-0227

Authors
Zender, Charles S.
Kiehl, J. T.

Publication Date
2012-09-21

DOI
10.1029/94JD02090

JOURNAL OF GEOPHYSICAL RESEARCH, VOL. 99, NO. D12, PAGES 25,869–25,880, DECEMBER 20, 1994

Radiative sensitivities of tropical anvils to small ice crystals

Charles S. Zender and J. T. Kiehl
National Center for Atmospheric Research, Boulder, Colorado

Abstract. Stratiform anvils in the upper tropical troposphere were simulated to determine the sensitivities of their radiative properties to the presence of small ice crystals. Cloud evolution was modeled in a one-dimensional (vertical) framework incorporating an updraft, deposition, sublimation, sedimentation, nucleation, and radiation. The sensitivities of cloud radiative forcing, albedo, emissivity, and heating rate were derived from a test that included and then excluded the presence of numerous small crystals. These crystals sizes ($3 < L < 20$ μm) have been measured in recent observations but are smaller than the detection limit of most past observations. The shortwave forcing and albedo were very sensitive to the presence of the small crystals, even though these crystals accounted for less than 2% of total cloud mass. For optically thick anvils the longwave forcing and emissivity were, in general, much less sensitive to the small ice crystals than their shortwave counterparts. Radiative treatments assuming a hexagonal crystal habit yielded the same sensitivities as the spherical habit. The results agreed with previous studies in that the increased backscatter from hexagonal crystals enhanced the planetary albedo by ~10–15%. The heating rate sensitivity to the small crystals depended on vertical location within the cloud and showed cancelation between the longwave and the shortwave heating perturbations. The small crystals changed heating rates by up to 50% at cloud top and base.

1. Introduction

Tropical cirrus anvils, formed by deep convective activity, play a crucial role in determining the Earth's radiation budget and climate. Cirrus anvils account for the most cloud cover over tropical oceans besides marine stratocumulus [*Warren et al.*, 1988] and their strong albedo effect [*Liou*, 1986] is possibly associated with the regulation of sea surface temperature and subsequent convective activity [*Ramanathan and Collins*, 1991]. Moreover, among all cloud types, they exist in the coldest part of the troposphere directly over the warmest oceans and thus produce the strongest greenhouse effect. The Earth Radiation Budget Experiment (ERBE) reveals that the net monthly radiation budget in the tropics is the small residual of a large cancelation between the countervailing longwave and shortwave effects of clouds [*Kiehl*, 1994].

To a first approximation the bulk cloud radiative properties observed by satellite are determined by the size distribution of hydrometeors, a difficult to observe microphysical quantity. Hence much work has been done on the inverse problem of determining cloud microphysical properties from the observed radiances. However, microphysical scale quantities such as condensate amount and hydrometeor size can vary significantly at space and timescales much finer than satellite resolution. Simulating the radiative budgets of cirrus as the size distribution changes throughout the growth, maintenance, and decay phases of the cirrus life cycle is only possible with high resolution, explicit microphysical models. A general circulation model (GCM), the chief tool for understanding the response of climate to cloud forcing, requires as input suitable spatial and temporal averages of these microphysical variations. The current accuracy of the effective ice crystal size input to GCMs can account for energy budget uncertainties exceeding the direct radiative forcing by anthropogenic greenhouse gases [*Coakley*, 1993]. The presence of undetected small-size ice crystals has been a continuing source of uncertainty and controversy in microphysical cirrus studies and hence in the GCMs which utilize predictions of crystal size from these studies.

Until recently, the lower detection limit (LDL) of in situ ice crystal measuring instruments has hovered around 20 μm [*Dowling and Radke*, 1990, hereinafter referred to as DR90]. Published measurements of ice crystal distributions, therefore, overestimated the mean size of crystals whenever there were (undetected) crystals smaller than the LDL present during the observations. Mie theory shows that crystals of length $L \sim 3$ μm are ~30% more efficient as scatterers (per unit area) than sizes $L \sim 20$ μm throughout the visible spectrum. Typically, crystals smaller than 50 μm account for well over 50% of cirrus crystal populations by number (but much less than 50% by mass) [*Heymsfield and Platt*, 1984, hereinafter HP84]. Their high optical efficiencies can dominate the scattering properties of the cloud. Neglecting (or extrapolating to) this important region of the size spectrum due to insufficient observational data can potentially effect calculated cloud radiative properties, notably albedo, emissivity, cloud forcing, and heating rates. It is therefore desirable to quantify the sensitivity of cirrus to small ice crystals in order to ascertain the accuracy of the radiative

Paper number 94JD02090.
0148-0227/94/94JD-02090$05.00

products derived from observations and subsequently used elsewhere, e.g., in climate models.

Data on crystal distributions in the tropics are rare, but recent work demonstrates that small crystals cannot be neglected in modeling. Using a combination of three instruments, *Knollenberg et al.* [1993, hereinafter KKW93] were able to measure a range of sizes from 0.1 to 2000 μm in the STEP tropical experiments. Their observations revealed that small crystals dominated the total crystal population by an order of magnitude or more in the cold tops ($-60 < T < -90$°C) of tropical cumulonimbus systems. (In this paper, crystals are denoted as small if the c-axis length is $L < 20$ μm, medium if $20 \leq L < 100$ μm, and large if $L \geq 100$ μm. The small category contains all those crystals undetectable by traditional instruments whose LDL is 20 μm.) Medium to large-size crystals accounted for ~90% of the mass whenever present. The measurements by *Heymsfield* [1986] of cirrus formed in gentle updrafts at the base of the cold tropical tropopause also point to an abundance of very small crystals ($L \sim 5$ μm) which often have been neglected in microphysical cloud models. The "typical cirrus" distribution given by DR90 was built mainly from midlatitude continental observations and yields far fewer small crystals than found by KKW93 for the same ice water content (IWC). This paper will examine the cloud radiative sensitivities to small ice crystals to estimate their importance in the overall radiative budget of tropical cirrus clouds.

Many studies have attempted to reconcile the optical properties of ice clouds with the observed microstructure. Because of the lack of measurements of cirrus crystal distributions in general and of small crystal sizes in particular, much of the effort has gone into analyzing the effects of the crystal habit (shape) on the radiative retrievals. The crystal habit must most often be inferred from a combination of other independent measurements. Information about the shape (e.g., aspect ratio) has been deduced from theoretical relationships between ice water content IWC and crystal concentration (KKW93) or IWC and radiance [*Paltridge and Platt*, 1981; *Stephens et al.*, 1990; *Stackhouse and Stephens*, 1991; *Baum et al.*, 1992]. When retrieved radiance is used to deduce habit, the fraction of backscattered radiation has been freely adjusted to match the modeled albedo with the observed. This adjustment has usually been made by decreasing the asymmetry parameter, g, the mean cosine of the photon scattering angle ($g = 1$ for complete forward scattering). It has long been known that the scattering phase function of a sphere of equivalent surface area tends to underestimate the amount of backscattered radiation relative to the true phase function of aspherical crystals [*van de Hulst*, 1957]. Only recently, however, has enough optical data become available on aspherical crystal habits to place any limits on the tuning of g to match model to observation. Because sufficient data on crystal habit and orientation in cirrus do not exist, it is premature to attempt to simulate the growth and maintenance of an actual cirrus anvil in every detail. Although not the primary focus of this paper, the radiative sensitivities of anvils to crystal shape could systematically mitigate or exacerbate the size sensitivities. This issue is briefly addressed by performing the same size sensitivity study for an anvil whose crystals are all radiatively treated as solid, randomly oriented hexagons, and then as spheres.

The approach to cirrus simulations taken by one-dimensional cloud modelers has been to examine macrophysical sensitivities to various microphysical processes in temporal and spatial regimes where dynamics is not thought to be a dominant forcing. Microphysical cirrus models in particular have been best suited to study quiescent kilometer-scale regions where the horizontal transport of moisture about the cloud might be small compared to the vertical. The synoptic regime in previous models has been detached anvils, orographically forced upliftings, and warm frontal overrunnings. *Zhang et al.* [1989, 1992] examined the effects of radiation, sedimentation, and vertical updrafts on cloud structure and maintenance. They found that although sedimentation lowered the cloud base, intense longwave heating (and subsaturation when present) caused sublimation which balanced the deepening of the cloud. *Jensen et al.* [1994b] recently performed sensitivity studies of continental cirrus to the nucleation mechanism, vertical updraft, and cloud height in a more general model framework that included aerosols.

We have developed and tested a one-dimensional microphysical cirrus model to perform tests of radiative sensitivities to crystal size. This study addresses the radiative sensitivities of tropical cirrus anvils to the presence of the small, hitherto undetectable crystals. The particular sensitivities of tropical anvils are of great importance to global climate modelers because of their role regulating the Earth's energy budget. The model employed the data of KKW93 to initialize a mature tropical anvil and then tracked the radiative properties through the anvil's slow decay. The radiative treatment of the crystals was performed with results from both Mie and hexagonal crystal theory. The study also examined how radiative uncertainties of tropical anvils caused by small ice crystals could influence our understanding of cloud maintenance and how the uncertainties compared to a doubled-CO_2 forcing.

The paper is organized as follows: Section 2 presents the details of the physical processes considered in the model and their numerical implementation. Section 3 details the control simulation of the tropical anvil and then presents the results of the sensitivity study to crystal size. The radiative sensitivities to be discussed are cloud forcing, albedo-emissivity relationships, and heating rate profiles. Section 4 discusses the size sensitivity in the framework of the model's limitations and current uncertainties in microphysical, cloud, and climate-scale processes. Section 5 concludes the paper with a summary of the results and their implications for future research.

2. Model Description

The dynamics and microphysical growth processes employed in this model substantially derived from the microphysical models of *Ramaswamy and Detwiler* [1986] and *Zhang et al.* [1992], so only the salient differences are detailed below.

2.1. Nucleation

Heymsfield and Sabin [1989] noted the lack of available ice-forming nuclei (IFN) and liquid water at cold temperatures ($T < -40$°C) and concluded that heterogeneous ice nucleation was unimportant in this region. They posited that homogeneous ice nucleation in deliquescent sulphate aerosols was responsible for most ice nucleation below −40°C

and found that homogeneous freezing of ammonium sulphate aerosol took place rapidly and within a narrow temperature range centered near −40°C. The rapid nucleation formed adequate deposition sites to deplete vapor availability and thus limit subsequent ice formation. Ammonium sulphate does not deliquesce until the relative humidity with respect to liquid water RH > 82%, so it probably causes no in situ nucleation in nonconvective upper tropospheric tropical cirrus.

A more probable nucleation site in the tropical upper troposphere is sulfuric acid which is wettable at any RH. *Jensen et al.* [1994a] found that H_2SO_4 ice-nucleating properties were very similar to ammonium sulphate. In accord with this we allowed the homogeneous freezing parameterization from *DeMott et al.* [1994], developed from ammonium sulphate data, to activate CCN at any RH in order to simulate the presence of either ammonium sulphate or sulphuric acid. The prescribed dry solute mass of the aerosol was a gamma distribution with a mean diameter of 0.075 μm. A modified version of *Meyers et al.* [1992] is employed for heterogeneous nucleation. Although these nucleation parameterizations were included in the model, the mechanisms were moisture limited in the part of the tropical upper troposphere examined in this study (11 < z < 18 km) and were never actually activated. KKW93 never measured ice saturation S_i > 110% from −90 < T < −50°C, so that RH < 70% in their observations. By varying the updraft speed in a mature anvil, it was found that liquid saturations exceeding 60% were unrealizable for T < −40°C without invoking convective strength updrafts (>1 m s^{-1}) which are uncharacteristic of stratiform cirrus. In short, there was no justification for the activation of any in situ ice nucleation mechanism in the mature tropical anvils colder than −50°C that were the subject of this study. The ramifications of actively nucleating anvils are further discussed in section 4.

2.2. Diffusional Crystal Growth

For reference the classical mass growth equation for an individual ice crystal falling in a vapor field employed here is

$$\frac{dm}{dt} = \left[4\pi C(S_i - 1 - \xi) - \frac{q_R l_s(\xi + 1)}{R_v T_\infty K f_T}\right] \cdot \left[\frac{R_v T_\infty}{D_v f_M e_i(T_\infty)} + \frac{l_s^2(\xi + 1)}{R_v T_\infty^2 K f_T}\right]^{-1} \quad (1)$$

where C is the shape factor, S_i is the saturation ratio with respect to ice, q_R is the radiative power absorbed by the ice crystal, T_∞ is the local environmental temperature, $\xi \approx 0$ is the curvature factor, and the other symbols are standard. Details of the derivation of (1) and the rest of the terminology may be found in the work of *Pruppacher and Klett* [1978].

Based on imaging of the moderate to large (L > 40 μm) crystals, KKW93 chose plates as the most likely crystal habit from their STEP observations. This deduction was in agreement with continental observations of habit at temperatures T < −50°C [*Heymsfield and Knollenberg*, 1972; *Heymsfield and Platt*, 1984]. The present study assumed all crystals were solid hexagons and prescribed an aspect ratio modified from *Auer and Veal* [1970]:

$$L/D = 5.82175 - 4.99677 \exp(L/500), \qquad L \text{ in } \mu\text{m} \quad (2)$$

The transition from plates to columns (L/D > 1) occurred at L = 20 μm.

2.3. Radiative Treatment

To complete the specification of the heat budget of an individual ice crystal, the radiative power q_R absorbed by each size crystal at every temperature was required each time step. The shortwave (SW) radiative transfer method employed was the δ-Eddington two-stream, 18-band model detailed by *Briegleb* [1992]. The solar zenith angle was chosen to be θ = 30° and the solar constant was 1370 W m^{-2}, so the downwelling top of the atmosphere (TOA) solar flux was 1186 W m^{-2}. The surface albedo was 0.1 for all solar bands at all angles to simulate the ocean. The longwave (LW) radiative transfer method employed was the CCM2 bulk absorptivity-emissivity method described by *Hack et al.* [1993]. In the cloudy region the schemes were modified to exclude gaseous absorption/emission which were very small compared to the flux divergence due to the ice crystals.

To gauge the possible effects of aspherical crystal habit in the radiative sensitivities, it was necessary to drop the spherical (Mie scattering) assumption. In this study we assumed the ice crystals were randomly oriented solid hexagonal crystals and employed the data of *Takano and Liou* [1989, hereinafter TL89] which has been used to model aspherical effects in other studies [e.g., *Ebert and Curry*, 1992; *Fu and Liou*, 1993].

The optical cross sections of hexagonal crystals were determined as follows: In the SW optical cross section, data were known from the TL89 model at five wavelengths of 0.7, 1.3, 1.9, 2.5, and 3.5 μm for each of five crystal sizes length/diameter (μm/μm) = 20/20, 50/40, 120/60, 300/100, and 750/160. The optical cross-sections σ_i, where i denotes scattering, absorption, or extinction, were specified relative to Mie theory. For spherical crystals, $\sigma_{\text{Mie},i} \equiv \pi r_s^2 Q_i$ where r_s is the radius and Q_i is the optical efficiency. Scaling parameters h_i were defined via

$$\sigma_{\text{hex},i} \equiv \sigma_{\text{Mie},i} h_i \quad (3)$$

where h_i was known at the 25 $\sigma_{\text{hex},i}$ data points and $\sigma_{\text{Mie},i}$ was computed for all sizes and wavelengths in advance. For arbitrary size and wavelength, $\sigma_{\text{hex},i}$ was computed by scaling $\sigma_{\text{Mie},i}$ by the closest known h_i in accord with (3). The hexagonal asymmetry parameter g was determined by the same method.

LW optical cross-section data for hexagonal crystals were only available in a distribution-integrated spectral format. Spectral cross-section data for a Cs size distribution [*Fu and Liou*, 1993] were known from the TL89 model for 12 spectral regions in the LW (K.-N. Liou, personal communication, 1992). The known LW Mie properties at arbitrary size and wavelength were then scaled by the appropriate spectral correction factor following the above procedure (3) and regridded onto the 31 LW bands internally carried by the model. From this information a mean LW Planck absorption coefficient $\bar{\kappa}$ was defined and employed to find the bulk LW cloud emissivity ε from [*Ebert and Curry*, 1992; *Hack et al.*, 1993]

$$\varepsilon = 1 - \exp(-\beta \bar{\kappa} \text{IWP}) \quad (4)$$

In implementing the above method for the TL89 SW data, it is important to ensure the computed asymmetry parame-

ter, coalbedo, and extinction cross section for hexagonal crystals were always less than those for equivalent spheres. The relative disparity between the hexagonal crystal properties and equivalent sphere properties must also decrease with increasing size parameter and aspect ratio. By adhering to these guidelines and employing (3), it was possible to produce a continuous distribution of hexagonal radiative properties from the limited scattering properties available. We found the radiative sensitivities of cirrus anvils to small crystals were not affected by the radiative treatment of the crystals as hexagonal shapes rather than spheres.

2.4. Growth Advection Scheme

The advection of the crystal distribution n through mass space by the growth process (1) was described by a continuity equation which ensured conservation of total number concentration N,

$$\frac{\partial n}{\partial t} = -\frac{\partial}{\partial m}\left(n\frac{dm}{dt}\right) \tag{5}$$

Finite differencing (5) is computationally stable when the Courant stability condition is met,

$$\Delta t < \frac{\alpha \Delta m}{(dm/dt)}, \qquad \alpha < 1 \tag{6}$$

where Δt is the time step, Δm is the width of the mass category, and α is a safety factor. Low-mass crystals ($L < 50$ μm) in the presence of moderate supersaturations s_i would have fast growth rates which violated the Courant condition (6) even for the smallest computationally feasible time steps. The hybrid procedure introduced by *Norville* [1990] was adopted to treat the equation by Lagrangian techniques for small masses and Eulerian techniques for large masses with a matching condition at the interface. A time step $\Delta t < 5$ s was chosen based on the quickest transport process, sedimentation of the largest crystals, and an $\alpha = 0.2$ safety factor for the $\Delta z \sim 75$ m vertical resolution. In each layer the region of the mass grid also stable for Δt-duration time steps was advected by the flux-corrected transport (FCT) method [*Oran and Boris*, 1987].

For the region of the mass grid where Δt would have been an unstable time step, a semi-Lagrangian technique was employed. The N_i crystals in each Lagrangian bin m_i were allowed to grow to a size $m' = m_i + \Delta t(dm_i/dt)$ where $m_j \le m' \le m_{j+1}$. Then the conditions of concentration and mass conservation were used to reapportion the N_i particles between the j and $j + 1$ mass bins according to

$$N_j = N_i \frac{m' - m_j}{m_{j+1} - m_j} \tag{7}$$

2.5. Grid Scaling and Crystal Geometry

A nonlinear mass grid was employed to preserve high resolution in the regime of small crystal sizes (where growth rates can be large) and to span the broad spectrum of sizes seen in the aircraft observations (HP84, KKW93).

The crystal mass was discretized according to

$$m_i = m_0 2^{(i-1)/2} \tag{8}$$

where m_i was the center point mass of the ith size bin and m_0 was the mass of a 3 or 20 μm particle for the control and truncated case, respectively. Fifty size bins were used for the control run, 35 for the truncated.

The particular habit is important in depositional, radiative, and collisional processes. The mass growth rate of a crystal (1) depends linearly upon its shape factor C, related to the surface area. The hexagonal geometry of ice plates and columns produces many of the visible optical phenomena associated with cirrus clouds (TL89). More detailed dependence of radiative factors upon crystal habit is discussed below. Finally, the collision rate among crystals (which is ignored in this paper) is proportional to their cross-sectional area.

The presence of a gentle mesoscale vertical updraft to supply vapor is crucial to capturing the longevity of cirrus in one-dimensional models. Without vapor transport processes, cirrus lifetime is limited by the sedimentation rate [*Zhang et al.*, 1992]. The total ice water path (IWP) scales linearly with the supersaturated vapor flux and thus with the updraft at small speeds. Such updrafts have been observed in continental [*Heymsfield*, 1977] and oceanic regimes [*Gamache and Houze*, 1983; *Leary and Houze*, 1980]. This model assumed a parabolic profile of vertical velocity $w(z)$ with a peak value $w_{\max}(z) = 5$ cm s^{-1} near $z = 14$ km. The updraft is allowed to advect water constituents but not dry air. It is implicitly assumed that any vertical convergence/divergence driven by the updraft profile is compensated by horizontal motion.

2.6. Prognostic Equation

The combined predictive equation for the evolution of the concentration $N_{i,k} = N(m_i, z_k)$ is written most concisely

$$\frac{\partial N_{i,k}}{\partial t} = -\left\{\Delta m_k \frac{\partial}{\partial m}\left[n_{i,k}\left(\frac{dm}{dt}\right)_{i,k}\right] + \frac{\partial}{\partial z}\left[(w_k + w_{\text{fall},i,k})N_{i,k}\right]\right\} + N_{\text{id}}\delta_{i,1} \tag{9}$$

where the subscripts i and k denote crystal size and altitude bins, respectively, and w_{fall} is the fall speed of the crystal taken from *Heymsfield* [1972]. The rate of production of ice crystal mass also appears as a sink term in the vertical continuity equation used to predict water vapor density. Except for the inclusion of the nucleation source term, this equation is identical to the concentration prognostic equation (2.1) in the work of *Zhang et al.* [1992].

2.7. Diagnostic Equations

A natural metric to compare the effects of changes in cloud structure on the environment is the spectral cloud forcing. Cloud forcing indicates the relative strengths of the albedo effect and the greenhouse effect of clouds. Although the cloud forcing indicates the important magnitude and sign of the cloud's net impact on the atmospheric column, climate modelers are also directly concerned with how the vertical profile of radiative heating rates is affected by clouds. Longwave cloud forcing (LWCF), shortwave cloud forcing (SWCF), net cloud forcing (NCF), and planetary albedo (A) were defined as follows:

$$\text{LWCF} = F_{\text{LW,clear sky}}(\tau = 0) - F_{\text{LW,cloud}}(\tau = 0),$$

$$\text{SWCF} = F_{\text{SW,clear sky}}(\tau = 0) - F_{\text{SW,cloud}}(\tau = 0), \quad (10)$$

$$\text{NCF} = \text{LWCF} + \text{SWCF}.$$

$$A = F^{\uparrow}_{\text{SW,cloud}}(\tau = 0)/F^{\downarrow}_{\text{SW,cloud}}(\tau = 0)$$

where $F^{\Updownarrow}$ are the upwelling and downwelling components of the radiative flux, F is the net upward flux ($F \equiv F^{\uparrow} - F^{\downarrow}$), and $\tau = 0$ is the top of the atmosphere (TOA). LWCF measures the longwave (LW) radiation trapped in the surface-atmosphere system due to clouds. Similarly, SWCF measures the difference in solar flux absorbed by the surface and atmosphere due to clouds. A more useful quantity to climatologists (available as archived satellite data), the diurnally averaged SWCF discussed below, is simply the daily mean SWCF. When NCF is negative, the presence of the clouds exerts a net cooling on the atmospheric column. It is well known that the cloud albedo strongly depends on IWP and the effective radius r_e of the crystal population, defined as the third moment of the crystal sizes divided by the second moment [*Slingo*, 1989; *Ebert and Curry*, 1992]:

$$r_e(z) \equiv \int_{r=0}^{r=\infty} \pi r^3 n(r, z)\, dr \Big/ \int_{r=0}^{r=\infty} \pi r^2 n(r, z)\, dr \quad (11)$$

For aspherical crystals the radius of the equivalent area sphere r_s was used in place of r in the integrand. The length of a hexagonal crystal described by (2) is approximately related to the radius of a sphere of equal area by $L \approx 2.5 r_s$. The integrated or mean cloud effective radius $\overline{r_e}$ is simply the vertical average of the number weighted $r_e(z)$.

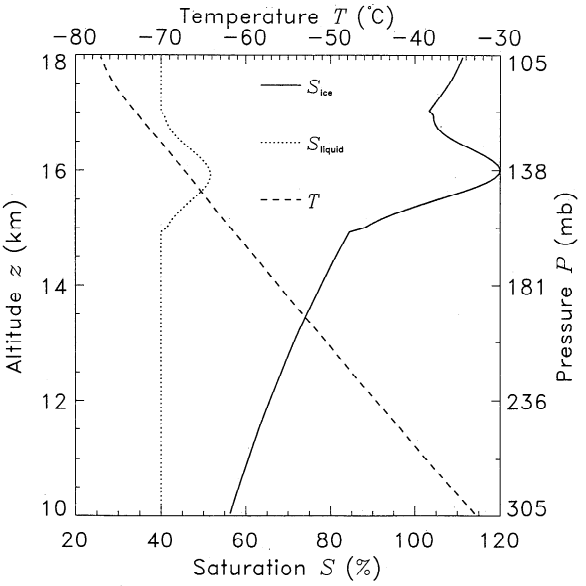

Figure 1. The initial environmental conditions of the cloud. Saturation with respect to ice water S_i (solid line), saturation with respect to liquid water S_l (dotted line), and temperature T (dashed line) as a function of the vertical coordinate.

Table 1. Initial and Final Properties of the Control Cloud and the Truncated Cloud

	Control	Truncated
Environmental profile	tropical	same
Distribution source	KKW93	same
Crystal habit	Hexagonal plates/columns	same
Minimum crystal length, μm	3	20
Cloud base, km	15	same
Cloud depth, km	2	same
Ice saturation S_i in cloud	1.2	same
Liquid saturation S_l outside cloud	0.4	same
Maximum vertical updraft $w_{\max}$, cm s^{-1}	5	same
Ice water path IWP, g m^{-2}	74.4 → 72.1	73.4 → 70.4
Mean ice water content $\overline{\text{IWC}}$, g m^{-3}	0.037 → 0.010	0.036 → 0.010
Mean concentration $\bar{N}$, L^{-1}	9580 → 2510	404 → 110
Mean effective radius $\overline{r_{\text{eff}}}$, μm	38.2 → 14.4	57.0 → 30.1
0.55 μm optical depth	5.6 → 6.3	3.7 → 3.8
Planetary albedo A	0.33 → 0.37	0.25 → 0.26
Cloud emissivity ε	0.98 → 0.98	0.95 → 0.95

The mean properties are vertical averages within the cloud. The change in prognosed quantities during an hour-long simulation is shown by the arrow.

2.8. Initial Conditions

Temperature and pressure and lower tropospheric moisture were taken from the tropical environmental profile adopted by the ICRCCM [*Luther et al.*, 1988]. Figure 1 shows the initial environmental conditions between 10 and 18 km. In this area the initial saturation ratio with respect to liquid water was specified to be $S_l = 40\%$ above and below the cloud, and a parabolic profile peaking at ice saturation $S_i = 120\%$ within the cloud. Therefore the environment was moister than the tropical troposphere on average but in closer agreement to the conditions which prevail during large cumulonimbus systems.

The initial ice crystal distribution was adapted from observations made in the anvil of a decaying tropical cyclone (KKW93, Figures 12 and 15). A factor which complicated the consideration of the very smallest crystals ($r_s < 1$ μm) was that the saturation vapor pressure drops relative to planar ice due to high surface curvature. This Kelvin effect can significantly enhance vapor deposition relative to thermal conduction and preclude the use of the classical depositional growth equation (1) which has been linearized to assume that conduction efficiently removes the latent heat generated by deposition [*Pruppacher and Klett*, 1978]. Counts recorded in the submicron range by the ASASX instrument did not distinguish between small ice crystals and IFN. Therefore only crystals larger than 3 μm (those which could have been counted by the FSSP and/or two-dimensional imaging probe) were considered in the model. The initial distribution of the cloud described in Table 1 is shown in Figure 2a.

To investigate the sensitivity of both the bulk radiative and the microphysical properties of an evolving cirrus cloud on the presence of small crystals, simulations both with and without the smallest crystals were performed. KKW93 found that approximately 80% of the crystals by number but

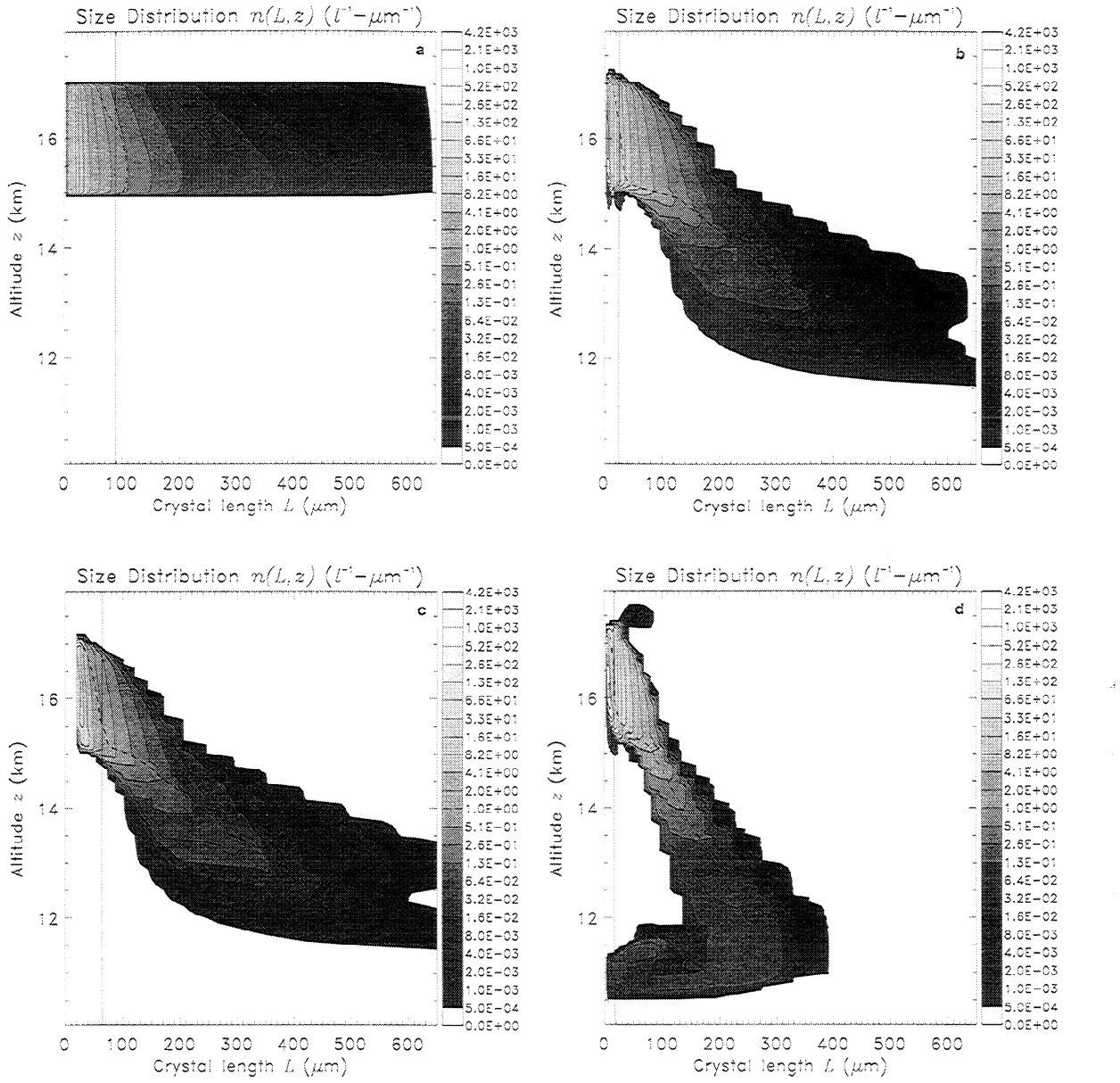

Figure 2. The ice crystal size distributions (m^{-3} μm^{-1}) used in the sensitivity study. Data are contoured geometrically (by factors of 2). The local effective length is indicated by the dashed curve; the vertical solid line represents the cloud-integrated or mean effective length. (a) The initial ice crystal distribution of the control cloud described in Table 1. Note the monotonic decrease of ice water content (IWC) and effective length with increasing altitude. (b) The control cloud in Figure 2a after one hour. (c) The truncated cloud (also described in Table 1) after one hour. Compare to Figure 2b. (d) The control cloud after four hours.

less than 5% by mass were located in the small crystal "tail," $3 \leq L < 20$ μm. The particular radiative sensitivities studied here were computed by taking the ratio of the results from the control run (which included the small crystals) to the "truncated" run, in which no crystals smaller than 20 μm were allowed. The smallest crystal in the simulation being 3 μm or 20 μm corresponded to modeling sizes resolved by KKW93 or in the numerous observations where LDL > 20 μm (DR89), respectively. Crystals whose equilibrium size in any time step became smaller than the LDL of the simulation (3 or 20 μm, respectively) were instantly and completely sublimated.

3. Results

The radiative sensitivity test described above was applied to the control cloud shown in Table 1. The truncated cloud was initialized exactly as the control cloud except that no crystals smaller than 20 μm were allowed. These small crystals accounted for about 1 g m^{-2} of the control cloud initially, less than 2% of total IWP. The truncation (or size) effect refers to the results that excising the small crystal tail had on the properties of the evolving truncated cloud. Before the results of the sensitivity test are presented, the behavior of the model is detailed for the control cloud itself.

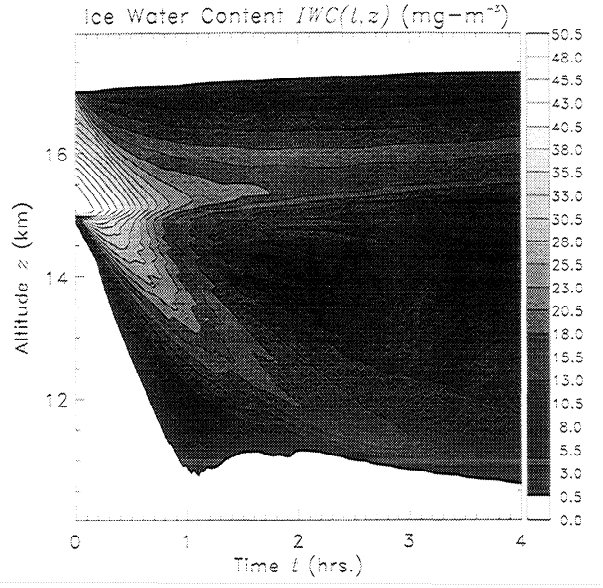

Figure 3. The evolution of IWC (g L^{-1}) from the control cloud in Table 1 and Figure 2a during 4 hours of evolution.

3.1. Evolution of the Control Cloud

The size distribution shown in Figure 2a was time advanced in 3 s dynamical and 15 s radiative time steps. The size distributions after 1 and 4 hours of integration are shown in Figures 2b and 2d, respectively, while the simultaneous evolution of IWC is illustrated in Figure 3. The main features of the evolution could be explained in terms of a competition between the rejuvenation of the cloud by the vertical updraft and the sublimation of sedimenting crystals. The updraft kept the small crystals aloft above the subsaturated air and prevented the complete dissolution of the cloud, which would have taken about 24 hours in still air. The evolution of the cloud could be characterized in five phases.

First was a ~3-min scavenging phase. IWP grew 1 g m^{-2} in a few minutes as crystals of all sizes commenced to feed off the initially supersaturated air (Figure 1) within the cloud. The ice mass deposition rate, $dm/dt \propto r$, favors the growth of the largest crystals present. However, most of the scavenged vapor accrued to small crystals (5–50 times less than 100 μm in radius) because they outnumbered the large crystals by O(1000). This depositional growth was too modest to affect $\overline{r_e}$ very much. The terminal fall speed of crystals length $L \sim 50$ μm was equal to the maximum updraft velocity, 5 cm s^{-1}. These "quasi-stationary" crystals underwent very little change in the 4 hours of evolution shown in Figures 2a, 2b, and 2d. Heavier crystals continuously fell out of the saturated region, diminishing the local $r_e(z)$ and causing $\overline{r_e}$ to shrink even as the cloud accumulated mass. The albedo A and emissivity ε both experienced their most rapid rates of growth during this period, owing both to the decrease in $\overline{r_e}$ and to the slight increase in IWP.

In the second phase, lasting until $t \sim 12$ min, the mass balance favored deposition from the updraft over subcloud sublimation though IWP grew only slowly. During this period both processes were relatively weak as the updraft did not cause any appreciable supersaturation nor had the heaviest crystals penetrated more than 0.5 km past the initial cloud base into the very subsaturated region. The maximum supersaturation $s_{i,\max}$ in any layer of the cloud had decreased from 20% to $s_{i,\max} < 1\%$ after ~5 min, so the environment was unable to sustain the initially rapid growth of the crystals in this phase. Crystals were still growing within the cloud, however, but their growth rates had come into equilibrium with the rate of vapor supply by the updraft. After the supersaturated vapor field was depleted, the change in mean effective radius was dominated by sedimentation and $\overline{r_e}$ began to asymptote from the initial 34 μm to an equilibrium value near 10 μm which it took about 4 hours to reach.

In the third phase, deposition became the stronger process as the updraft conveyed moister air from below into the cloud more quickly than sublimation removed mass. During $10 < t < 30$ min, the cloud added another 1 g m^{-2} of ice, and reduction of $\overline{r_e}$ was decelerated. During this time the heaviest crystals had fallen almost to $z = 13$ km, where $S_i \sim 70\%$.

In the fourth phase, from $30 < t < 60$ min, the cloud entered the sublimation-dominated period of decreasing IWP but had not yet established its equilibrium cloud base. By this time the heaviest crystals had reached 12 km, $S_i \approx 65\%$. The vapor pressure gradient from the crystal to the environment at this moisture level was large enough to sublimate the IWP by ~10 g m^{-2} h^{-1}. The effective radius had declined to 15 μm but began to level off as fewer crystals were still sublimating. Sublimation had considerably narrowed the size distribution in the hour between Figures 2a and 2b.

The fifth phase describes the period of anvil decay between the establishment of the cloud base near $z = 11$ km until the end of the simulation ($1 < t < 4$ hours). The remnants of the heaviest crystals reached the eventual cloud base near $z = 11$ km, $S_i = 60\%$ after about two hours, having fallen about 1 m s^{-1} most of the way. The large sedimenting crystals (sometimes known as virga) sublimated completely before reaching 10 km. The quick sublimation in this dry air was marked by the slightly distended lobe in Figure 3 at $t = 1$ hour. The slow vertical transport of water vapor and small crystals from below maintained IWC in the top of the cloud after $t > 1$ hour. The mean crystal length stabilized near 17 μm, and the IWP leveled off near to the 50 g m^{-2}. During this period the IWP was nearly equally partitioned between the saturated region of the cloud above 15 km and the sublimating region beneath 15 km.

Figure 2d shows a pronounced crystal gap from the height where the virga disappeared near 11 km to the base of the main cloud at 15 km. No crystals between $0 < L < 100$ μm existed in the gap because none of the crystals heavy enough to sediment into the gap had time to completely sublimate there. Of course, when sublimating crystals became smaller than 50 μm, they were lifted by the updraft to a less subsaturated region, prolonging their lifetime. Extended integrations (not shown) confirmed that this hydrologic cycle could be maintained indefinitely in the closed model system and that mass sedimentation beneath 10 km was negligible.

3.2. Sensitivity of Size Crystal Distribution

The size distributions of the control and truncated (Figures 2b and 2c) clouds show very similar morphology after an hour's evolution. The effective radius of the truncated cloud was everywhere about 20 μm larger than in the control cloud due the absence of the large numbers of small crystals.

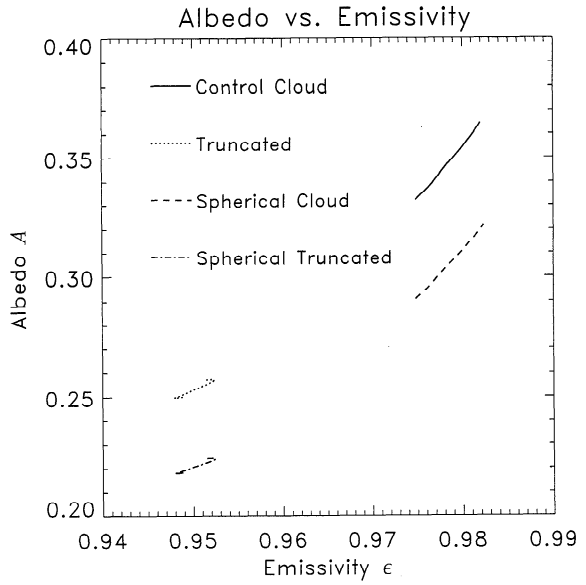

Figure 4. The albedo and emissivity are tracked through time for the control (solid line) and truncated clouds (dotted line). Time increases along the curves from the bottom left to the top right. Shown for comparison are the results of radiatively treating the ice crystals as spheres of equivalent surface area with Mie theory, the spherical control (dashed line) and spherical truncated (dotted-dashed line) simulations. The reflectance of the spheres is much less, but the sensitivity to truncation is very close to the hexagonal case. The initial ice water path was ~74 g m^{-2} in all four cases.

Since the very hygroscopic small crystals were not present, the mass of the initially supersaturated vapor was deposited over a broader and larger range of sizes. An examination of the mass distribution (mg m^{-3} μm^{-1}) of the two cases showed most of the mass (~1 g m^{-2}) of the initially supersaturated vapor ended up in crystals $L < 50$ μm in the control case, and $L < 120$ μm in the truncated case. The center of mass of the truncated cloud was lower in elevation because of all the mass carried in larger crystals.

3.3. Sensitivity of Albedo and Emissivity

The decay of the anvil and its IWP during most of the simulation did not decrease A or ε in the control case. On the contrary, the decrease of $\overline{r_e}$ and the increase of κ (equation (4)) overcompensated the decreasing IWP throughout the simulation and enhanced A and ε, respectively. In the truncated case, however, the artificial limit of $L = 20$ μm prevented large relative changes in $\overline{r_e}$, so A and ε commenced decreasing soon after the IWP peaked.

Figure 4a compares the shape sensitivity to the truncation sensitivity in albedo-emissivity phase space for the first hour of the simulation. The shape sensitivity was determined using Mie theory instead of the radiative treatment for the aspherical crystals discussed in section 2.3, so the clouds are labeled "spherical." The ratio of the control cloud properties to the truncated cloud properties was nearly identical for each of the two distinct radiative treatments of crystal habit. Thus the sensitivities to crystal truncation were independent of crystal shape for the case of single-habit clouds composed of randomly oriented crystals examined here.

As expected, both size and shape effects tended to underestimate the albedo of the control cloud. The bias in albedo caused by treating the crystals as spheres was about 0.05 in absolute terms, a 15% sensitivity. The bias in albedo due to the truncation effect was about 0.1, a 30% sensitivity. The trend in the albedo bias was to slowly increase with time as the effective lengths of the two clouds decreased during the anvil decay.

3.4. Sensitivity of Cloud Forcing

Up to now, only instantaneous forcings have been examined. To evaluate the climatic significance of the modeled tropical anvils, the diurnally averaged LWCF and SWCF are considered. The diurnally averaged SWCF presented in Figure 5 was specified as π^{-1} (the daily mean of cos θ) times the local noontime SWCF. The truncation effect decreased the albedo enough to increase NCF by ~40 W m^{-2}. The truncation effect caused a smaller change in LWCF than in SWCF because the emissivity of both cases was nearly unity (saturated). Although both clouds had nearly identical IWP, truncation of the smallest crystals caused a significant bias (decrease) in the absorption coefficient κ, and hence ε (equation (4)). When the IWP was small enough so that the emissivity $\varepsilon \ll 1$, simulations revealed greater LWCF sensitivities than shown here.

3.5. Sensitivity of Heating Rates

Optically thick clouds are characterized by sharp changes in flux profiles, so a small change in the absorption properties of a given distribution of condensate can result in significant local changes in heating rates. The profiles presented in Figure 6 refer to instantaneous rather than diurnally averaged heating rates. The profiles between $1 < t < 4$ hours were not significantly different from Figure 6b. As expected in optically thick cloud tops, the LW cooling exceeded SW absorption. Surface thermal emission absorbed at cloud base caused the heating maximum. The

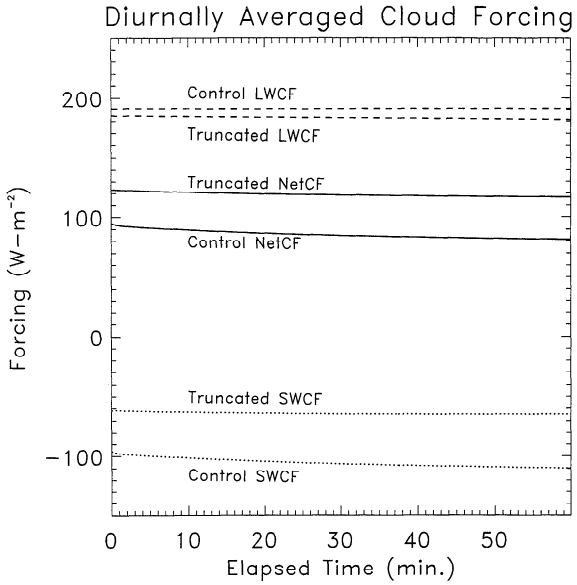

Figure 5. The time evolution of the diurnally averaged cloud forcings (W m^{-2}) of the control and truncated clouds described in Table 1. Shortwave cloud forcing (short dashes), longwave cloud forcing (long dashes), and net cloud forcing (solid line).

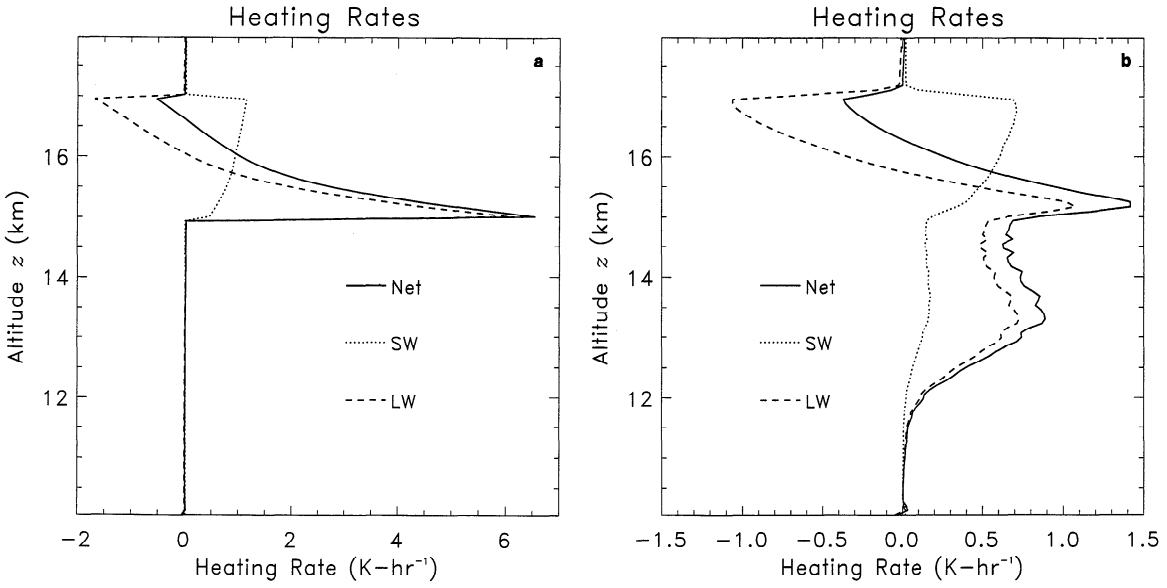

Figure 6. Vertical profiles of instantaneous radiative heating rates (°K h^{-1}) from the control tropical anvil. Shown are the shortwave heating rate (short dashes), longwave heating rate (long dashes), and net heating rate (solid line). (a) The initial heating rates corresponding to Figure 2a. (b) The heating rates after one hour corresponding to Figure 2b.

initial cloud base heating rate of 6°K h^{-1} quickly weakened because the differential sedimentation of the largest crystals smeared out the flux gradient over a larger vertical distance.

The SW heating rate was sensitive to the presence of crystals with strong absorption peaks in the near infrared (NIR). KKW93 noted particularly the importance of solar absorption at 3.0 μm for small crystals at cloud top. They showed with Mie theory that the absorption efficiency for ice spheres is sharply peaked near $\lambda = 3$ μm for crystal sizes $1 < r_s < 8$ μm. This 3-μm peak is roughly independent of crystal shape because the absorption efficiency is most dependent on the index of refraction and the size parameter. In agreement with KKW93 the bias in SW heating in Figure 7 peaked at cloud top where the total number concentration, not the IWC, was a maximum (compare Figures 2 and 3). This clearly demonstrates the importance of their findings of large numbers of small ice crystals at cloud top.

The SW heating rates further into the cloud were very

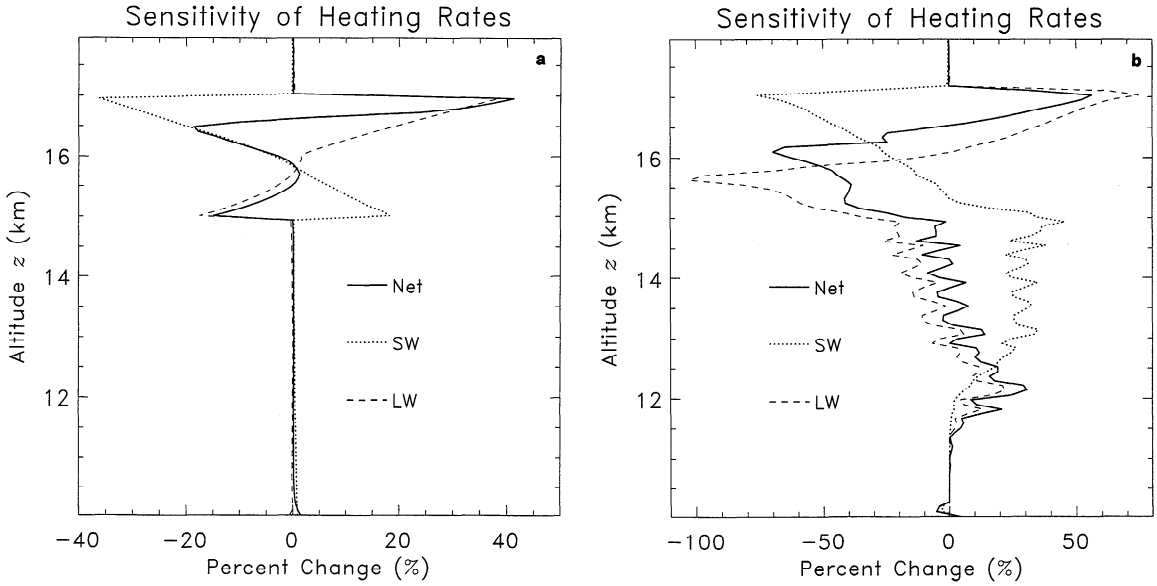

Figure 7. The sensitivity of the local heating rates to the small crystals is expressed as a relative percentage difference between the heating rates in the control cloud (shown in Figure 6) and in the truncated cloud (not shown). The sensitivity was forced to zero where the control cloud heating rate was less than 0.1°K h^{-1} in order to filter out large ratios due to small numbers. (a) The heating rate sensitivity at the initial conditions. (b) The heating rate sensitivity after an hour.

sensitive to the truncation effect. Interestingly, Figure 7 shows that truncating the crystal distribution enhanced SW heating everywhere beneath cloud top. The underlying cause of the enhanced heating in the lower regions of the anvil was the decreased albedo of the truncated cloud. In the visible band the single-scattering albedo was very near unity but the flux was large, while the converse was true in the NIR. The small crystals in the control cloud had significantly attenuated the NIR flux before it could reach cloud base. More downwelling and upwelling (surface reflected) visible and NIR flux was therefore responsible for the extra absorption in the lower regions of the truncated cloud.

Crystals smaller than 20 μm are also highly efficient absorbers in the LW bands. Their absence presented a "cleaner" IR window to transmitted radiation from below, which decreased cloud base heating in the truncated cloud. Near cloud top where the average crystal size was the smallest, truncation reduced IR emission because there were fewer emitters, as measured by number, mass, and surface area.

The net heating difference correlated with the LW heating anomaly because the magnitude of LW heating was nearly everywhere greater than the SW heating (Figure 6). The SW heating bias was largely anticorrelated with the LW heating bias (Figure 7). At nighttime this cancelation of biases is absent and the net heating bias would equal the LW bias in Figure 7.

4. Discussion

The results of the sensitivity tests have shown that radiative properties of the truncated cloud are not adequate substitutes for those of the control cloud. However, the truncated cloud did not deviate very much from the control cloud in the directly measurable microphysical quantity IWP. The radiative biases were largely due to the misrepresentation of the effective radius due to the truncation effect. The specification of $\overline{r_e}$ from the current database of cirrus observations will likely introduce more error (than the IWP) in mesoscale and global-scale models.

The largest uncertainties in the model were the specification of the nucleation rate, the absence of horizontal transport and convection, and the assumption of the crystal habit. As previously mentioned, the tropical upper troposphere studied here was too cold, vapor poor, and IFN depleted to activate either the homogeneous or the heterogeneous freezing mechanisms. Actively nucleating clouds, however, would be expected to have even larger truncation sensitivities. For example, an activated IFN appearing at $L = 20$ μm would consume 32 times the vapor and scatter only 7 times the radiation as an IFN activated at $L = 3$ μm. The LDL of the truncated cloud, 20 μm, was about 5 μm too large to resolve the equilibrium effective length of the control cloud. The truncation sensitivity would have diminished in an environment favoring larger crystals, such as a stronger updraft, as long as nucleation was still negligible.

The updraft speed in the present study was chosen because it was comparable to the largest monthly mean updrafts in the upper tropical troposphere. The nucleation processes of sulphate aerosols must be better understood before the present model can be applied to tropical cirrus in regions above 50–60% RH. The truncation sensitivity of actively nucleating anvils would be exacerbated if the nucleation were fast enough, so that the competition among small crystals for vapor suppressed the growth of large crystals. *Jensen et al.* [1994b] predicted the effective radius of cirrus crystals would decrease with increasing updraft velocity.

The model did capture many of the observed features of stratiform clouds without employing any parameterized diffusion, convection, or entrainment. For example, the correlation between temperature and IWC and r_e noted by HP84 was seen in the model. However, the model was unequipped to handle superadiabatic lapse rates which developed so that only microphysical processes could dissipate the convectively available potential energy of a parcel. The current one-dimensional model is too simple to generalize any results to dynamically active conditions. A two-dimensional version of this model and/or a diffusional parameterization of heat and mixing would ensure that any convective instabilities generated at cloud top and base could be damped by dynamical (as well as microphysical) processes. The resulting entrainment would alter the life cycle of the crystals and could have significant implications for crystal sizes at cloud edges.

To isolate the radiative sensitivities, the hexagonal/spherical distinction was maintained only in the radiative portion of the model. All crystals were treated as hexagonal in computing the shape factor C and the ventilation factors f_M and f_T in (1). The spherical ice habit had greater thermal and mechanical diffusivity than the hexagonal habits and $C_{\text{sphere}} \approx 1.5 C_{\text{column}}$ [*Pruppacher and Klett*, 1978; *Heymsfield*, 1972]. These microphysical differences tended to slow the growth of aspherical crystals relative to equivalent area spheres. Slower growth enhanced the importance of the radiative heating of the crystal relative to the latent heating. *Mitchell* [1994] demonstrated that including a temperature dependence to ice crystal habit can significantly effect the evolved size distribution of simulated midlatitude continental cirrus.

The radiative heating contribution to an ice crystal's energy budget has been shown to dominate latent and sensible heating at cloud top [*Stephens*, 1983]. Because of the dependence of the crystal single-scattering properties on habit it was necessary to make assumptions about crystal habit before attempting to simulate radiative budgets of tropical anvils. The hexagonal crystals assumed this model did not cause as great a change in albedo (Figure 4) as reported by *Stephens et al.* [1990] and *Stackhouse and Stephens* [1991]. The main reason for this discrepancy was their choice of $g = 0.7$ which corresponded to crystals of a considerably different shape than those considered here. They found that changing the value of the asymmetry parameter from the Mie value ($g \approx 0.87$ in the visible) to $g = 0.7$ nearly doubled the cloud albedo independent of cloud emittance. The TL89 model showed that g decreased with decreasing aspect ratio L/D from 0.85 (at $L = 750$ μm, $L/D = 4.7$) to 0.77 (at $L = 20$ μm, $L/D = 1$) in the visible part of the spectrum for hexagonal crystals. Since g decreased with aspect ratio, careful calculation of g for randomly oriented hexagonal plates or dendrites ($L/D < 1$) could result in a g nearer 0.7 which would reconcile the discrepancy.

The radiative results of accounting for aspherical habits (i.e., lowering g) are hard to distinguish from the results obtained by including more small crystals (i.e., decreasing the effective radius, r_e). Both changes lead to more back-

scattering and increased extinction optical depths. However, a point not emphasized in the literature is that adding small crystals increases total absorption, while treating crystals as hexagons decreases total absorption. The implication is that observed flux divergences could prove useful in determining whether crystal size, or shape, or both needed tuning to match model results to theory. It was shown that the truncation sensitivity of the anvils in Figure 4 was independent of the choice between spheres and hexagons for radiative shape. Theoretical studies of the optical properties of other aspherical crystal habits in the manner of TL89 are needed to more fully address the radiative and thermodynamic feedbacks of crystal size and shape both on the evolution of single clouds and on the kinds of cloud ensembles resolved by global-scale models.

This model can be used to obtain a crude estimate of the importance of the truncation sensitivity relative to potential climate forcings. The uncertainty in the diurnally averaged surface energy balance due to distribution truncation was ~ 40 W m^{-2} (Figure 5). The zonal annual average amount of cirriform clouds above tropical oceans from surface observations is ~15% [*Warren et al.*, 1988]. If the control cloud were assumed to be a "typical" tropical cirrus, then neglecting the smallest crystals could account for a ~ 4 W m^{-2} overestimate of the tropical (mainly daytime surface) energy budget. This is equivalent in magnitude but opposite in sign to the predicted instantaneous radiative forcing of a doubling of CO_2 (a diurnal effect felt mainly in the atmospheric column) [*Shine et al.*, 1990]. The same net effect occurs for an ~2% change in total cloud albedo over the tropics, or an ~1% change in the solar constant.

The truncation effect caused changes in the local flux divergences which were large compared to the energy needed to sublimate the cloud. The local heating biases in Figure 7 amount to diurnally averaged variations in LW and SW heating of up to 5 and 10°K d^{-1}, respectively. It would only take the dissipated power of 4°K d^{-1}, entirely converted into the latent heat of sublimation, to sublimate an anvil with IWC < 0.1 g m^{-3} within an hour. Typical lifetimes of tropical anvils, however, are about 6 hours [*Ackerman et al.*, 1988], and many anvils take longer to dissipate.

5. Conclusion

Improved understanding of the radiative balance in tropical anvils is essential to forecasting energy budgets in the tropical atmosphere. A radiative sensitivity study was performed by changing to the smallest size of ice crystal resolved by the model to match the LDL representative of the older and newer generation of available cirrus observations. This paper has demonstrated persistent changes in heating rates, albedos, and cloud forcings >10% result from not representing the small crystals $L < 20$ μm in clouds of a given IWC.

The truncation sensitivity was independent of crystal shape, at least for solid hexagonal crystals and spheres. The implications of unobserved small ice crystals in cirrus observations are probably comparable to or more serious than uncertainties about crystal shape. The truncation sensitivity of cirrus albedo was large, and the absence of small crystals appreciably reduced SWCF. Anvil emissivity ε and LWCF were fairly insensitive to truncation for opaque cirrus. The truncation sensitivity of local heating rates was highly variable throughout the anvil. The net sensitivity showed that cancelation between the LW and the SW sensitivities was important, especially at cloud top and base. Better knowledge of crystal habit (e.g., improved imaging probes) can be used to constrain r_e. Conversely, more reliable r_e can be used to constrain crystal habit. Using either size or shape as a free "tunable" parameter to match observations is unlikely to work for both reflectance and heating rates at the same time.

Distribution-resolving microphysical models point toward the difficulty of accurately representing crystal distributions with bulk microphysics. The exact partitioning of given IWC seems to be important, at least at small crystal sizes. The small crystal truncation sensitivity test uniformly excised less than 2% of ice mass (IWC), yet the heating rates at cloud top and cloud base were changed by up to 50%. One- or two-parameter analytic fits to crystal distributions (e.g., gamma functions) are often employed in the bulk microphysical models which are used at mesoscales and larger scales. In conjunction with observations, distribution-resolving microphysical models can address the problem of picking the fewest parameters possible to achieve a given level of accuracy in light of the radiative sensitivities.

The results of the sensitivity test performed indicate to what degree the size effect may be neglected in microphysical (and by extension larger scale) cloud and climate models. The demonstrated sensitivities of the bulk radiative properties serve to advocate improvements to the LDL of observations of crystal size distributions. More size distribution parameterizations from tropical and maritime cirrus observational campaigns such as CEPEX and ARM are essential to assessing the climatological importance of small ice crystals. Further observations in conjunction with microphysical modeling efforts are needed to remove some of the uncertainties currently embedded in the parameterization of cirrus in large-scale models.

Acknowledgments. The authors wish to thank Y. Takano and K.-N. Liou for graciously providing the results of their hexagonal ice crystal model, S. Warren for making his index of refraction data available, G. Taylor for providing the FCT code, and B. Briegleb for providing a bulletproof SW radiation code. This work was supported in part by Earth Observing System project W-17,661. The National Center for Atmospheric Research is sponsored by the National Science Foundation.

References

Ackerman, T. P., K.-N. Liou, F. P. J. Valero, and L. Pfister, Heating rates in tropical anvils, *J. Atmos. Sci.*, *45*(10), 1606–1623, 1988.

Auer, A. H., Jr., and D. L. Veal, The dimension of ice crystals in natural clouds, *J. Atmos. Sci.*, *27*, 919–926, 1970.

Baum, B. A., B. A. Wielicki, P. Minnis, and L. Parker, Cloud-property retrieval using merged HIRS and AVHRR data, *J. Appl. Meteorol.*, *31*, 351–369, 1992.

Briegleb, B. P., Delta-Eddington approximation for solar radiation in the NCAR community climate model, *J. Geophys. Res.*, *97*, 7603–7612, 1992.

Coakley, J. A., Jr., Remote sensing of cloud microphysics, paper presented at Summer Colloquium on Clouds and Climate, 27 pp., Natl. Cent. for Atmos. Res., July 5–23, Boulder, Colo., 1993.

DeMott, P. J., M. P. Meyers, and W. R. Cotton, Parameterization and impact of ice initiation processes relevant to numerical model simulations of cirrus clouds, *J. Atmos. Sci.*, *51*(1), 77–90, 1994.

Dowling, D. R., and L. F. Radke, A Summary of the Physical

Properties of Cirrus Clouds, *J. Appl. Meteorol.*, *29*, 970–978, 1990.

Ebert, E. E., and J. A. Curry, A parameterization of ice cloud optical properties for climate models, *J. Geophys. Res.*, *97*, 3831–3836, 1992.

Fu, Q., and K.-N. Liou, Parameterization of the Radiative Properties of Cirrus Clouds, *J. Atmos. Sci.*, *50*, 2008–2025, 1993.

Gamache, J. F., and R. A. Houze Jr., Water budget of mesoscale convective system in the tropics, *J. Atmos. Sci.*, *40*, 1835–1850, 1983.

Hack, J. J., B. A. Boville, B. P. Briegleb, J. T. Kiehl, P. J. Rasch, and D. L. Williamson, Description of NCAR community climate model (CCM2), *NCAR Tech. Note*, *NCAR/TN–382+STR*, 108 pp., Natl. Cent. for Atmos. Res., Boulder, Colo., 1993.

Heymsfield, A., Ice crystal terminal velocities, *J. Atmos. Sci.*, *29*, 1348–1357, 1972.

Heymsfield, A. J., Precipitation development in stratiform ice clouds: A microphysical and dynamical study, *J. Atmos. Sci.*, *34*, 367–381, 1977.

Heymsfield, A. J., Ice particle evolution in the anvil of a severe thunderstorm during CCOPE, *J. Atmos. Sci.*, *43*(21), 2463–2478, 1986.

Heymsfield, A. J., and R. G. Knollenberg, Properties of cirrus generating cells, *J. Atmos. Sci.*, *29*, 1358–1366, 1972.

Heymsfield, A. J., and C. M. R. Platt, A parameterization of the particle size spectrum of ice clouds in terms of the ambient temperature and the ice water content, *J. Atmos. Sci.*, *41*(5), 846–855, 1984.

Heymsfield, A. J., and R. M. Sabin, Cirrus crystal nucleation by homogeneous freezing of solution droplets, *J. Atmos. Sci.*, *46*(14), 2252–2264, 1989.

Jensen, E. J., O. B. Toon, D. L. Westphal, S. Kinne, and A. J. Heymsfield, Microphysical modeling of cirrus, 1, Comparison with 1986 FIRE IFO measurements, *J. Geophys. Res.*, *99*, 10421–10442, 1994a.

Jensen, E. J., O. B. Toon, D. L. Westphal, S. Kinne, and A. J. Heymsfield, Microphysical modeling of cirrus, 2, Sensitivity studies, *J. Geophys. Res.*, *99*, 10443–10454, 1994b.

Kiehl, J. T., On the observed near cancellation between longwave and shortwave cloud forcing in tropical regions, *J. Clim.*, *7*, 559–565, 1994.

Knollenberg, R. G., K. Kelly, and J. C. Wilson, Measurements of high number densities of ice crystals in the tops of tropical cumulonimbus, *J. Geophys. Res.*, *98*, 8639–8664, 1993.

Leary, C. A., and R. A. Houze Jr., The contribution of mesoscale motions to the mass and heat fluxes of an intense tropical convective system, *J. Atmos. Sci.*, *37*, 784–796, 1980.

Liou, K.-N., Influence of cirrus clouds on weather and climate processes: A global perspective, *Mon. Weather Rev.*, *114*, 1167–1199, 1986.

Luther, F. M., R. G. Ellingson, Y. Fouquart, S. Fels, N. A. Scott, and W. J. Wiscombe, Intercomparison of radiation codes in climate models (ICRCCM): Longwave clear-sky results—A workshop summary, *Bull. Am. Meteorol. Soc.*, *69*(1), 40–48, 1988.

Meyers, M. P., P. J. DeMott, and W. R. Cotton, New primary ice-nucleation parameterizations in an explicit cloud model, *J. Appl. Meteorol.*, *31*, 708–721, 1992.

Mitchell, D. L., A model predicting the evolution of ice particle size spectra and radiative properties of cirrus clouds, I, Microphysics, *J. Atmos. Sci.*, *51*(6), 797–816, 1994.

Norville, K. W., A study of the ice-hail charge separation mechanism using a thunderstorm electrification model with explicit microphysics in a kinematic framework, Ph.D. dissertation, 99 pp., Dep. of Atmos. Sci., Univ. of Wash., Seattle, Wash., 1990.

Oran, E. S., and J. P. Boris, *Numerical Simulation of Reactive Flow*, 601 pp., Elsevier Science, New York, 1987.

Paltridge, G. W., and C. M. R. Platt, Aircraft measurements of solar and infrared radiation and the microphysics of cirrus cloud, *Q. J. R. Meteorol. Soc.*, *107*, 367–380, 1981.

Pruppacher, H. R., and J. D. Klett, *Microphysics of Clouds and Precipitation*, 433 pp., D. Reidel, Norwell, Mass., 1978.

Ramanathan, V., and W. Collins, Thermodynamic regulation of ocean warming by cirrus clouds deduced from observations of the 1987 El Niño, *Nature*, *351*, 27–32, 1991.

Ramaswamy, V., and A. Detwiler, Interdependence of radiation and microphysics in cirrus clouds, *J. Atmos. Sci.*, *43*(21), 2289–2301, 1986.

Shine, K. P., R. G. Derwent, D. J. Wuebbles, and J.-J. Morcrette, Radiative forcing of climate, in *Climate Change, The IPCC Scientific Assessment*, edited by J. T. Houghton, G. J. Jenkins, and J. J. Ephraums, pp. 45–68, Cambridge University Press, New York, 1990.

Slingo, A., A GCM parameterization for the shortwave radiation properties of water clouds, *J. Atmos. Sci.*, *46*(10), 1419–1427, 1989.

Stackhouse, P. W., and G. L. Stephens, A theoretical and observational study of the radiative properties of cirrus: Results from FIRE 1986, *J. Atmos. Sci.*, *48*(18), 2044–2059, 1991.

Stephens, G. L., The influence of radiative transfer on the mass and heat budgets of ice crystals falling in the atmosphere, *J. Atmos. Sci.*, *40*, 1729–1739, 1983.

Stephens, G. L., S.-C. Tsay, P. W. Stackhouse, and P. J. Flatau, The relevance of the microphysical and radiative properties of cirrus clouds to climate and climatic feedback, *J. Atmos. Sci.*, *47*(14), 1742–1753, 1990.

Takano, Y., and K.-N. Liou, Solar radiative transfer in cirrus clouds, I, Single-scattering and optical properties of hexagonal ice crystals, *J. Atmos. Sci.*, *46*(1), 3–19, 1989.

van de Hulst, H. C., *Light Scattering by Small Particles*, 470 pp., Dover, Mineola, N. Y., 1957.

Warren, S. G., C. J. Hahn, J. London, R. M. Chervin, and R. L. Jenne, Global distribution of total cloud cover and cloud type amounts over the ocean, *NCAR Tech. Note*, *NCAR/TN–317+STR*, 150 pp., Natl. Cent. for Atmos. Res., Boulder, Colo., 1988. (Available as *NTIS DE90-003187*, Natl. Tech. Inf. Serv., Springfield, Va.)

Zhang, Y., M. Laube, and E. Raschke, Numerical studies of time behaviour of cirrostratus in still air, *Beitr. Phys. Atmos.*, *62*(4), 307–320, 1989.

Zhang, Y., M. Laube, and E. Raschke, Evolution of stratiform cirrus simulated in a lifting layer, *Beitr. Phys. Atmos.*, *65*(1), 23–34, 1992.

J. T. Kiehl and C. S. Zender, National Center for Atmospheric Research, P. O. Box 3000, Boulder, CO 80307-3000.

(Received September 8, 1993; revised August 3, 1994; accepted August 11, 1994.)